Nano Research
DOI 10.1007/s12274-013-0354-2
Research Article
ISSN 1998-0124
CN 11-5974/O4

Enhanced performance of GaN nanobelt-based photodetectors by means of piezotronic effects

Ruomeng Yu[1,§], Caofeng Pan[2,§], Youfan Hu[1], Lin Li[3], Hongfei Liu[4], Wei Liu[5], Soojin Chua[4], Dongzhi Chi[4], and Zhong Lin Wang[1,2] (✉)

[1] *School of Materials Science and Engineering, Georgia Institute of Technology, Atlanta, Georgia 30332-0245, USA*
[2] *Beijing Institute of Nanoenergy and Nanosystems, Chinese Academy of Sciences, Beijing, China*
[3] *School of Physics, Georgia Institute of Technology, Atlanta, Georgia 30332, USA*
[4] *Institute of Materials Research and Engineering, A*STAR (Agency for Science, Technology, and Research), Singapore 117602, Singapore*
[5] *School of Electrical and Electronic Engineering, Luminous! Center of Excellence for Semiconductor Lighting and Display, Nanyang Technology University, Singapore 639798, Singapore*
[§] *These authors contributed equally to this work.*

Received: 4 July 2013
Accepted: 28 July 2013

KEYWORDS

GaN nanobelts, Schottky contact, piezotronics, photodetector

ABSTRACT

GaN ultraviolet (UV) photodetectors (PDs) have attracted tremendous attention due to their chemical stability in harsh environments. Although Schottky-contacted GaN-based UV PDs have been implemented with better performance than that of ohmic contacts, it remains unknown how the barrier height at local Schottky contacts controls the sensors' performance. In this work, the piezotronic effect was employed to tune the Schottky barrier height (SBH) at local contacts and hence enhance the performances of Schottky-contacted metal–semiconductor–metal (MSM) structured GaN nanobelt (NB)-based PDs. In general, the response level of the PDs was obviously enhanced by the piezotronic effect when applying a strain on devices. The responsivity of the PD was increased by 18%, and the sensitivity was enhanced by from 22% to 31%, when illuminated by a 325 nm laser with light intensity ranging from 12 to 2 W/cm^2. Carefully studying the mechanism using band structure diagrams reveals that the observed enhancement of the PD performance resulted from the change in SBH caused by external strain as well as light intensity. Using piezotronic effects thus provides a practical way to enhance the performance of PDs made not only of GaN, but also other wurtzite and zinc blende family materials.

1 Introduction

Visible-blind ultraviolet (UV) photodetectors (PDs) have drawn tremendous attention during the past decades after finding wide applications in numerous fields such as solar UV monitoring, flame detection,

Address correspondence to zhong.wang@mse.gatech.edu

biological sensing and engine tracking [1–4]. GaN, as an important Ⅲ–Ⅴ semiconductor material with direct wide band gap, has been widely reported for fabricating various visible-blind PDs due to its outstanding chemical stability as well as visible blindness [5–9]. However, the performance of ohmic-contacted GaN visible-blind UV PDs is retarded by their low response speeds, relatively long reset times and limited sensitivity [10–13]. To increase the detection efficiency and optimize the working principle, Schottky contacts have been introduced into GaN visible-blind UV PDs [14–18], and this can provide high sensitivity, impressive response and reset times as well as good detection limits, because the Schottky barrier height (SBH) at the local contact will effectively dominate the performance by controlling the transport process when reversely biased [19]. However, it remains unclear how to tune the barrier height and obtain an optimal SBH, in order to obtain the most enhanced PD performance.

The piezotronic effect, found in piezoelectric semiconducting materials (such as GaN, ZnO, and CdS), provides an effective way to tune the SBH at the metal–semiconductor (MS) interface by utilizing the piezoelectric polarization charges produced at a surface/interface when under an externally applied strain, and can work as a strain "gate" to control the electron transport process of the devices [20]. It has been proved that piezotronic effects can significantly enhance the performance of light emitting diodes (LEDs) [21, 22], solar cells [23, 24], and bio/chemical sensors [25, 26].

In this work, piezotronic effects were employed to optimize the SBH and thus enhance the performance of Schottky-contacted metal–semiconductor–metal (MSM) structured GaN nanobelt (NB)-based PDs. In general, the response level of PDs was obviously enhanced by piezotronic effects when applying strain to devices. The optimized external strain, indicating an optimal SBH at MS contact, was found to be –0.53%, at which the responsivity of the PD was increased by 18%. The sensitivity of GaN NB-based PDs was enhanced by from 22% to 31% under a –0.53% compressive strain, when illuminated by a 325 nm laser with light intensity ranging from 12 to 2 W/cm^2. The physical mechanism behind the observed optoelectronic behavior was carefully studied using band structure diagrams, which account for the change in SBH resulting from tuning the external strains and light intensity leading to the enhanced performances of PDs. Using piezotronic effects thus provides a practical way to enhance the performance of PDs made not only of GaN, but also other wurtzite family materials.

2 Experimental

GaN NBs were synthesized via strain-controlled cracking of thin solid GaN film as reported elsewhere [27]. The as-obtained GaN NBs were well separated with lengths of several hundreds of micrometers and widths of around 10 μm, indicative of anisotropic nanostructures, as shown in Fig. 1(a). A high resolution transmission electron microscopy (HRTEM) image and the corresponding selected area electron diffraction (SAED) pattern (Figs. 1(b) and 1(c)) also confirm that the GaN NB is a single crystal and that its polar *c*-axis lies along the longitudinal direction of the NB. The PD was fabricated by transferring and bonding an individual GaN NB laterally on a polystyrene (PS) substrate (of 500 μm in thickness) with its *c*-axis in the plane of the substrate. Silver paste was employed to fix both ends of the GaN NB and serve as source and drain electrodes, forming a MSM structure. A thin layer of polydimethylsiloxane (PDMS) was applied to package the PD, aiming at not only improving the mechanical robustness of the whole device, but also preventing it from contamination and corrosion by gas or moisture in the ambient atmosphere. The optical image of an as-fabricated GaN NB-based PD is presented in Fig. 1(d) (inset). The experimental set-up, as shown in Fig. 1(d), includes two 3D stages with movement resolution of 1 μm to introduce compressive/tensile strains on the device and a beam of laser simultaneously illuminating at a certain spot. The magnitude and the sign of applied strains can be calculated following the method reported elsewhere [28].

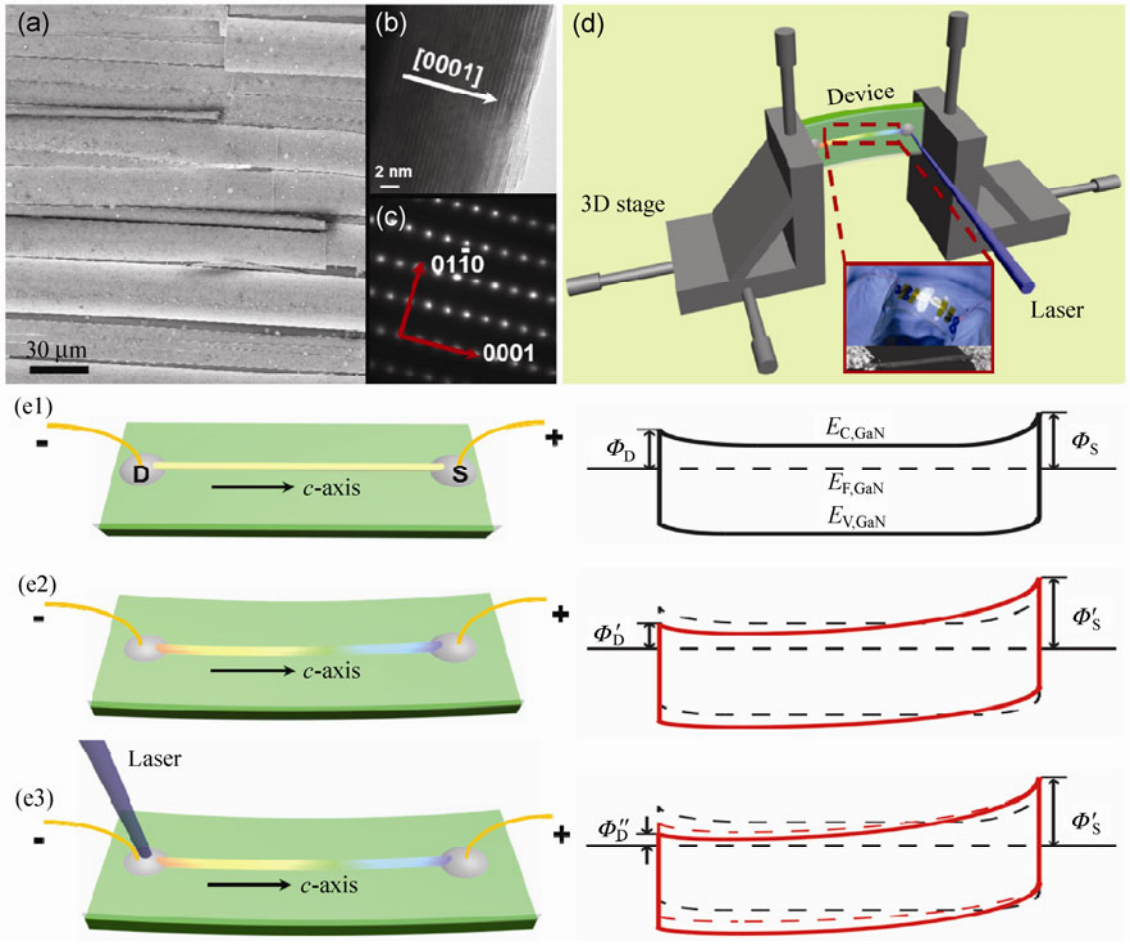

Figure 1 (a) SEM image of GaN NBs. (b) HRTEM image of a GaN NB and (c) the corresponding SAED pattern of the same GaN NB. (d) Experimental setup and optical images of the as-fabricated PD (insets). (e) The band structure of the GaN NB-based PD under different conditions to demonstrate the working principle. The crystallographic *c*-axis of the NB runs from drain to source as labeled. (e1) Schematic and band structure of a strain-free device (presented as a black solid line in (e1), black dashed line in (e2) and (e3)), where the drain electrode was reversely biased. (e2) Schematic and band structure of a compressively strained device (presented as a red solid line in (e2), red dashed line in (e3)), where the drain electrode was reversely biased. (e3) Schematic and band structure of a compressively strained device with laser illumination at the drain electrode (presented as red solid line in (e3)), where the drain electrode was reversely biased.

3 Theoretical basis

The physical mechanism of the GaN NB-based PDs is illustrated using band structure diagrams shown in Fig. 1(e). A strain-free GaN NB (Fig. 1(e1)) forms Schottky contacts of different barrier heights (Φ_D and Φ_S) with metal electrodes at both ends. The electron transport process of the PD is dominated by the reversely biased Schottky contact [19], which is the drain electrode in this case. Once the substrate is bent, a compressive/tensile strain is created in the NB since the mechanical behavior of the entire device is determined by the substrate [28]; this strain will produce a distribution of piezopotential along the *c*-axis, with its polarity depending on the crystallographic orientation of GaN and the sign of the strain (Fig. 1(e2)) [29]. A negative piezopotential at the semiconductor side effectively increases the local SBH, while a positive piezopotential reduces the barrier height. When the GaN NB-based PD is under compressive strain (Fig. 1(e2)), SBH at the reversely biased drain contact is reduced by the strain-induced positive piezopotential, which gives rise to an increased current in the device. If a laser beam is simultaneously focused

at the drain electrode, as presented in Fig. 1(e3), the SBH at the drain contact will be reduced even further, since more electron–hole pairs are generated upon laser illumination and the injection of electrons into the conduction band of GaN effectively increases the charge carrier density of the whole device and, correspondingly, an increase in current is expected.

4 Results and discussion

By applying a series of compressive strains on the GaN NB-based PD, *I*–*V* characteristics of a single PD were derived as a function of the strain as shown in Fig. 2(a). A clearly asymmetric electromechanical behavior in current response to strain at both electrodes was obtained under a triangular wave swiping from –2 to +2 V across the device, as dictated by the piezotronic effect. This confirms the electron transport process of the PD was dominated by piezotronic effects, an interfacial effect asymmetrically tuning the local contact characteristics, rather than piezoresistive effects, which are a symmetric volume effect without polarity. The data of $|I|$ vs. strain at –2 V and +2 V are plotted in the inset of Fig. 2(a). The band structure

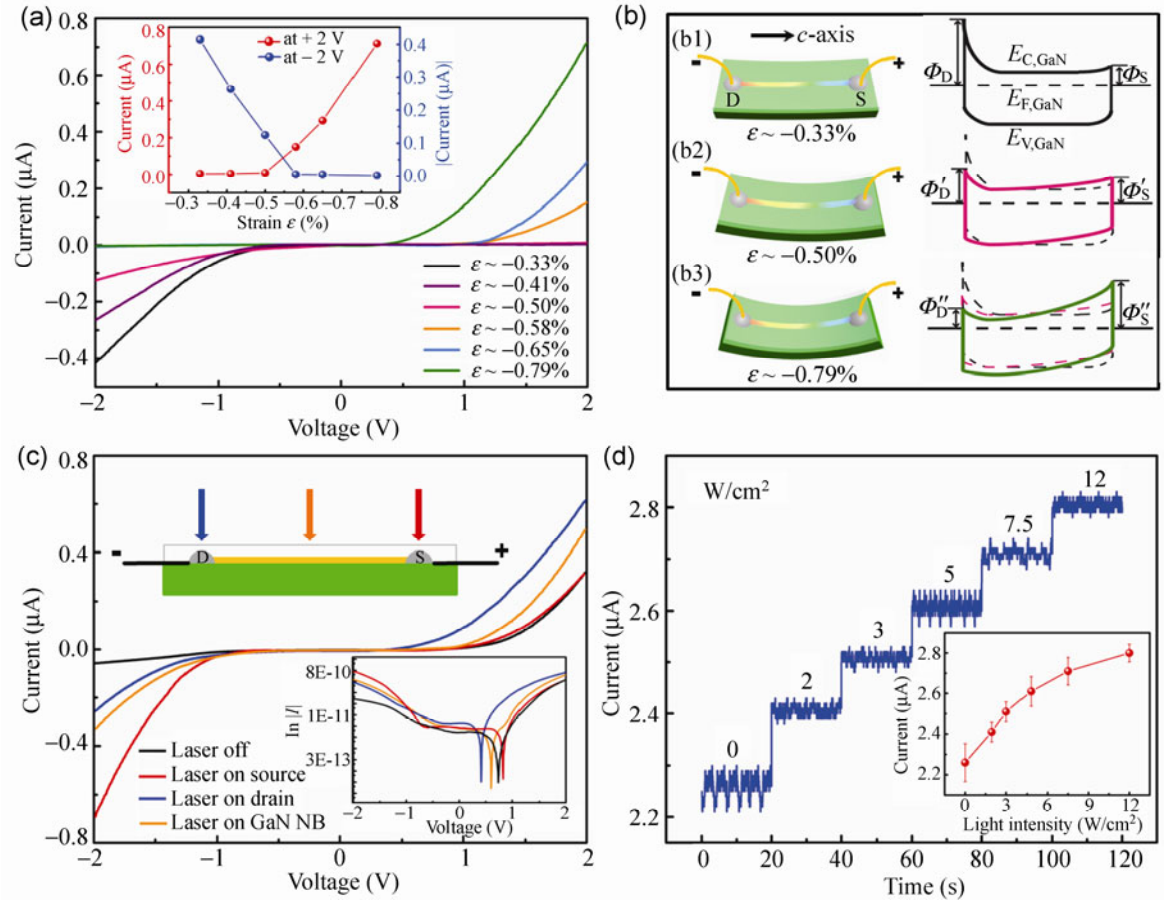

Figure 2 (a) *I*–*V* characteristics of a GaN NB-based PD under a series of compressive strains, with a triangular wave swiping from –2 to +2 V across the device. The inset is the plot of $|I|$ vs. strain at –2 V and +2 V. (b) Band structure illustrating the *I*–*V* characteristics of a GaN NB-based PD shown in (a), with the crystallographic *c*-axis of the NB running from drain to source as labeled. (b1) Schematic view and band structure of a device under –0.33% compressive strain (presented as a black solid line in (b1), black dashed line in (b2) and (b3)). (b2) Schematic view and band structure of a device under –0.50% compressive strain (presented as a pink solid line in (b2), pink dashed line in (b3)). (b3) Schematic view and band structure of a device under –0.79% compressive strain (presented as an olive solid line in (b3)). (c) *I*–*V* characteristics and schematic view (inset) of a strain-free GaN NB-based PD under 5 W/cm^2 laser illumination on the source electrode, GaN NB or drain electrode, with a triangular wave swiping from –2 to +2 V across the device. The inset is the plot of ln $|I|$ vs. voltage. (d) *I*–*t* characteristics of a strain-free GaN NB-based PD under different 325 nm laser light intensities focused on the drain electrode, which was reversely biased at a fixed 2 V. The inset is the corresponding *I* vs. light intensity curve.

diagrams of GaN-based PDs are presented in Fig. 2(b) to illustrate the observed *I*–*V* characteristics shown in Fig. 2(a). By swiping a triangular wave from –2 to +2 V across the device, the drain electrode was reversely biased at the $V > 0$ side, while the source electrode was reversely biased at the $V < 0$ side, as shown schematically in Fig. 2(b). According to the proposed working principles of GaN NB-based PDs demonstrated in Fig. 1(e), externally applied compressive strains produced a positive piezopotential at the drain electrode, and a negative piezopotential at the source electrode. Therefore, the SBH was reduced step by step at the drain electrode, while the SBH at the source electrode was increased when applying a series of compressive strains on the PD. This provides a good explanation for the *I*–*V* characteristics presented in Fig. 2(a).

The response of GaN NB-based PD to laser illumination at different spots was derived by separately shining the 325 nm laser at the drain electrode, the middle of the GaN NB and the source electrode (inset of Fig. 2(c)), with a triangular wave swiping from –2 to +2 V across the device. *I*–*V* characteristics of the device shown in Fig. 2(c) indicate clearly that, when the laser was focused on the source electrode, the current increased significantly under a bias voltage ranging from –2 to –1 V, in which case the source electrode was reversely biased; a similar increase was also observed for laser illumination at the drain electrode. This shows that the current of GaN NB-based PDs will be enhanced as long as the laser illuminates the reversely biased electrode. When the laser was focused on the GaN NB, the current of the device increased at both ends, with smaller increases in magnitude compared to those when shining the laser on the drain electrode or source electrode. The observed optoelectronic behavior agrees very well with the above physical mechanism proposed for GaN NB-based PDs. Since laser illumination at the reversely biased electrode can effectively reduce the local SBH, which dominates the electron transport process of the whole device, it therefore has a more significant influence on the PD current than in the case when more electron–hole pairs were merely generated inside the conducting channel when the laser was focused on the GaN NB. A plot of ln $|I|$ vs. voltage is presented in the inset of Fig. 2(c), in which opposite trends of current under forward and reverse biases are apparent, which is a typical characteristic of the piezotronic effect.

With the drain electrode of a strain-free PD reversely biased at a fixed voltage of 2 V, *I*–*t* characteristics were obtained as a function of light intensity as presented in Fig. 2(d). Obvious increases in current were observed on increasing the light intensity from 0 to 12 W/cm^2, with the beam of the 325 nm laser precisely illuminating the drain electrode. *I* vs. light intensity data extracted from the *I*–*t* characteristics are plotted in the inset of Fig. 2(d). The reproducibility and stability of the GaN NB-based PDs were also investigated as shown in the Electronic Supplementary Material (ESM) (Fig. S1).

By systematically investigating the response of GaN NB-based PDs to a series of strains as well as light intensities with the drain electrode reversely biased at a fixed voltage of 2 V under a 325 nm beam laser illuminating at the drain electrode, a 3-dimensional (3D) surface plot was derived (Fig. 3(a)) by extraction from the data plotted in Figs. 3(b)–3(g). A straightforward overall trend in the current of the PD on changing either the strain or light intensity can easily be concluded from Fig. 3(a), and is consistent with the *I*–*t* characteristics presented in Figs. 3(b)–3(g) that either larger strain or higher light intensity lead to a higher response current of the PD.

To optimize the performance of GaN NB-based PDs, the relative changes in response current with respect to externally applied strain and 325 nm laser light intensity are plotted as another two 3D surface graphs in Figs. 4(a) and 5(a). The absolute and relative current response of GaN NB-based PDs to various light intensities when the compressive strain was fixed, ranging from –0.00% to –0.71%, are presented in Figs. 4(b) and 4(c), respectively. As can be seen from Fig. 4(b), the response current of the PD at very weak light intensity was increased by applying a –0.71% compressive strain, in which case an enhancement in the detection limit of the device by as much as 44% was achieved. From the relative current response to light intensity shown in Fig. 4(c), it seems that the largest relative change in current was obtained with no strain applied. However, the current output signal

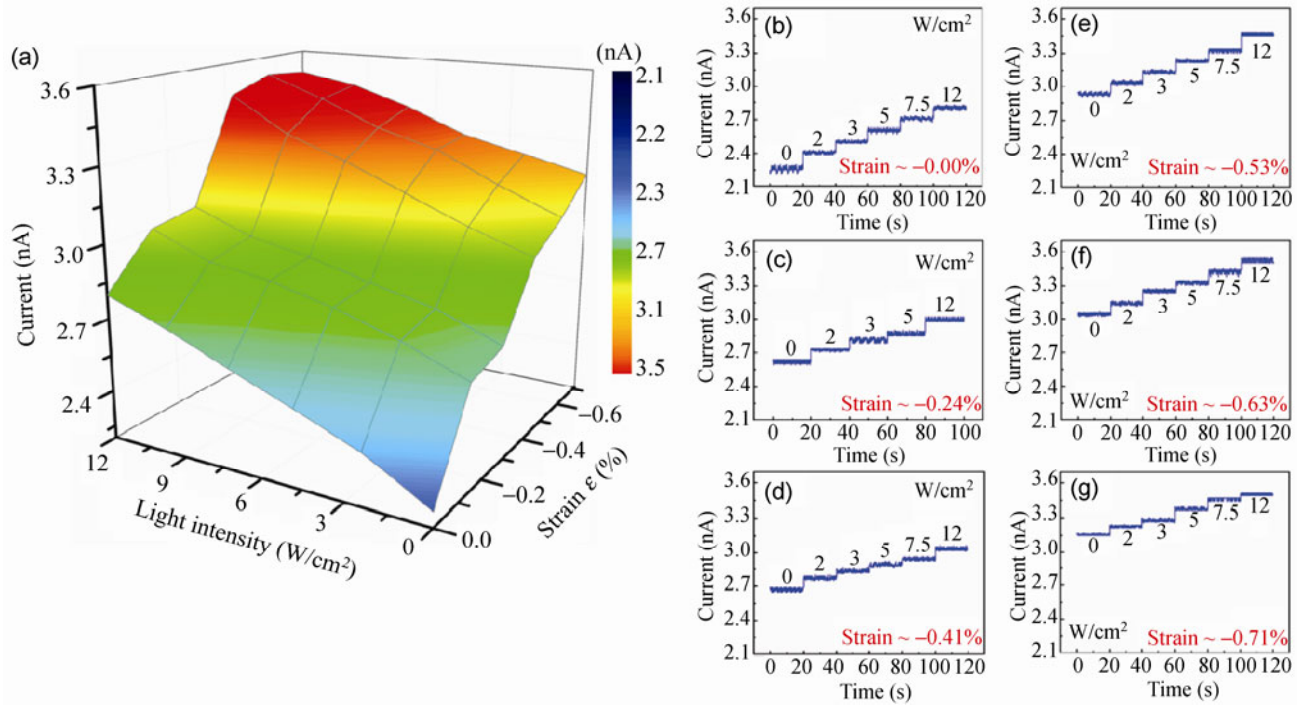

Figure 3 (a) 3D surface graph illustrating the current response of a GaN NB-based PD to strain and light intensity. *I*–*t* characteristics of a GaN NB-based PD with 325 nm laser illumination on the drain electrode, which was reversely biased at a fixed 2 V, with light intensity ranging from 0 to 12 W/cm^2 under a compressive strain of (b) –0.00%; (c) –0.24%; (d) –0.41%; (e) –0.53%; (f) –0.63%; (g) –0.71%.

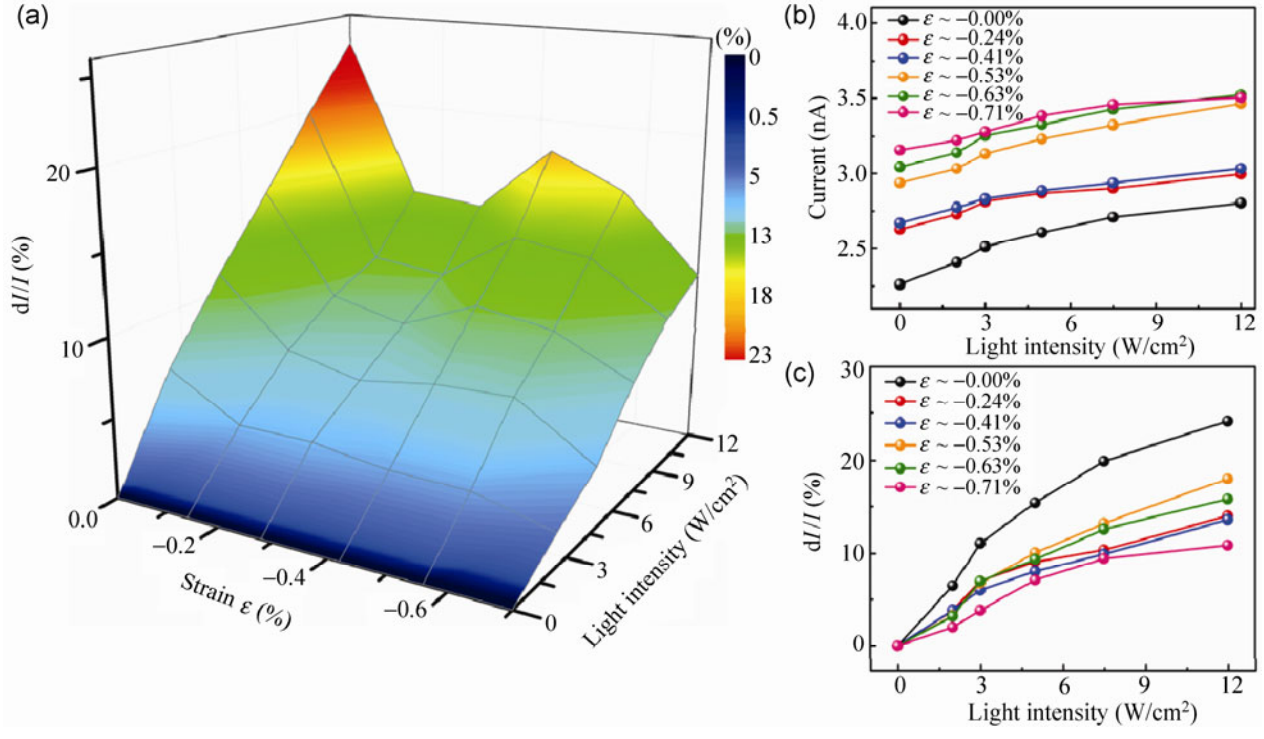

Figure 4 (a) 3D surface graph illustrating the relative change of current of a GaN NB-based PD with respect to strain (*x*-axis) and light intensity (*y*-axis), with 325 nm laser illumination on the drain electrode, which was reversely biased at a fixed 2 V. (b) Absolute and (c) relative current response of a GaN NB-based PD under different light intensities, with compressive strain ranging from –0.00% to –0.71%.

at extremely low light intensity was too weak to be detected by the system when no external strain was applied. Considering both the restriction of detection limit and the responsivity, the best performance of the GaN PD was achieved under –0.53% compressive strain (the yellow line in Fig. 4(c)) rather than under strain-free conditions; under this optimized externally applied strain, the responsivity of the PD was enhanced by 18%. An explanation can be proposed to address the reason why the optimized strain was –0.53% instead of the highest strain of –0.71%. Since high light intensity may generate a large number of electron–hole pairs, which could accumulate and cause the strain-induced polarization charges to be partially screened, the efficacy of positive piezopotential in reducing the SBH might decrease with increasing light intensity. This screening effect may lead, at some point, to no increase in response current when applying higher strain under a relatively high level of light illumination. On the other hand, the response current under weak light illumination is still significantly enhanced by applying more strain. Therefore the relative change in response current did not increase monotonically with externally applied strain, but with an optimized performance at a strain of –0.53% as observed. This hypothesis can also be confirmed from the observed "platform" (high light intensity and high strain region) in Fig. 5(a), which clearly shows the lack of increasing response current with increasing strain under high illumination intensities. The absolute and relative current responses of GaN NB-based PDs to various strains when the light intensity was fixed, ranging from 0 to 12 W/cm^2, are presented in Figs. 5(b) and 5(c), respectively. By externally applying a compressive strain of –0.71% to the device, the sensitivity of the PD was observed to increase by 27%–40% when the light intensity ranged from 12 to 2 W/cm^2.

5 Conclusions

The piezotronic effect has been employed to tune the SBH and hence enhance the performance of Schottky-contacted MSM structured GaN NB-based PDs. In general, the response level of the PDs was

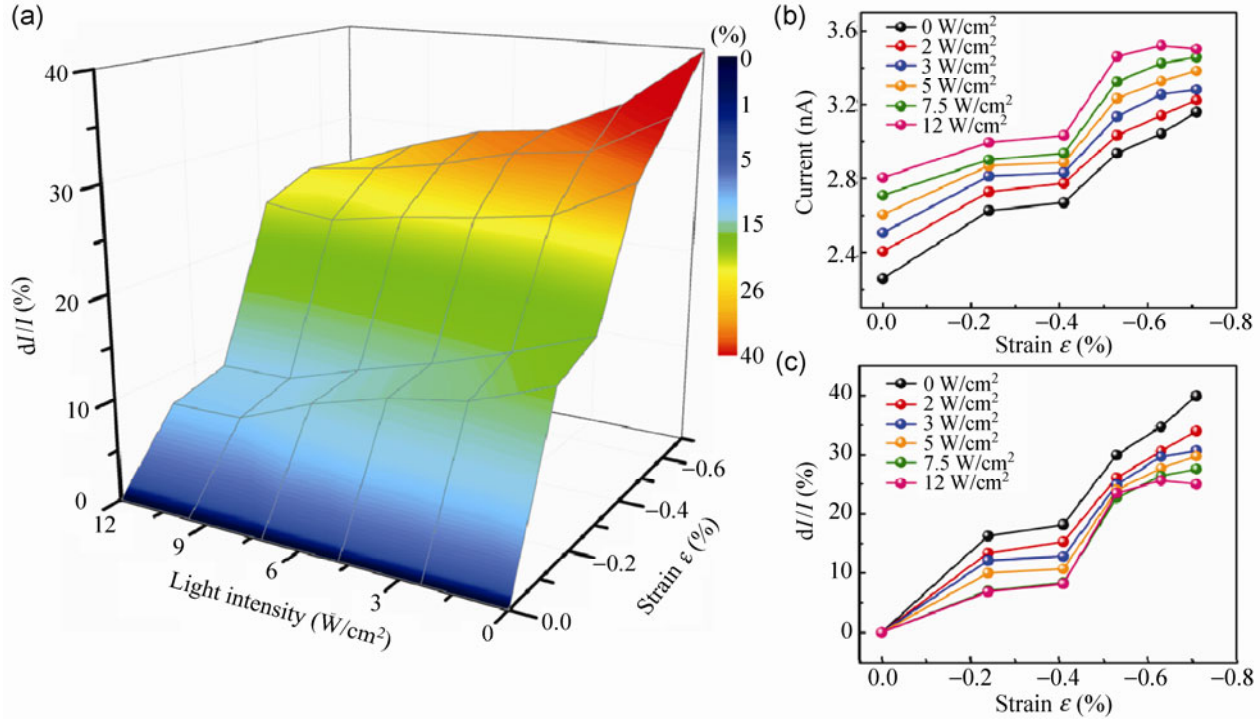

Figure 5 (a) 3D surface graph illustrating the relative change of current of a GaN NB-based PD with respect to light intensity (*x*-axis) and strain (*y*-axis), with 325 nm laser illumination on the drain electrode, which was reversely biased at a fixed 2 V. (b) Absolute and (c) relative current response of a GaN NB-based PD under different compressive strains, with light intensities ranging from 0 to 12 W/cm^2.

obviously enhanced by the piezotronic effect when applying a series of strains on devices. The optimized external strain, indicating an optimal SBH at MS contact, was found to be –0.53%, at which the responsivity of the PD was increased by 18%. The sensitivity of GaN NB-based PDs was enhanced by 22% to 31% under a –0.53% compressive strain, when illuminated by a 325 nm laser with light intensity ranging from 12 to 2 W/cm^2. The physical mechanism behind the observed optoelectronic behavior was carefully investigated using band structure diagrams. The changes in SBH resulting from tuning the external strain as well as the light intensity accounted for the enhanced performances of GaN NB-based PDs. Using piezotronic effects thus provides a practical way to enhance the performances of PDs made not only of GaN, but also other wurtzite family materials.

Methods

Synthesis and characterization of GaN NBs. GaN NBs were derived by strain-controlled cracking of thin solid GaN films. The as-fabricated GaN NBs were characterized by scanning electron microscopy (SEM) (LEO FESEM 1550 and LEO FESEM 1530), transmission electron microscopy (TEM) (JEOL-JEM 4000) with selected area diffraction (SAD), and HRTEM (FEI F30) with energy-dispersive X-ray spectroscopy (EDX).

Fabrication of GaN NB-based PDs. The PD was fabricated by transferring and bonding an individual GaN NB laterally on a polystyrene (PS) substrate (of 500 mm in thickness) with its *c*-axis in the plane of the substrate. Both ends of the GaN NB were fixed by silver paste, which also served as source and drain electrodes. A thin layer of PDMS was applied to package the PD.

Experimental setup for GaN NB-based PDs. A synthesized function generator (Model No. DS345, Stanford Research Systems, Inc.) and a low-noise current preamplifier (Model No. SR570, Stanford Research Systems, Inc.) were used for electrical measurements. The strains were introduced by using two three-dimensional mechanical stages with a movement resolution of 1 mm face to face locking the PD in the middle. A He–Cd laser (wavelength = 325 nm, Model No. KI5751I-G, Kimmon Koha Co., Ltd.) was illuminated at certain locations of the device. The performances of the device were measured by a computer-controlled measurement system.

Acknowledgements

This research was supported by National Science Foundation (NSF), Multidisciplinary University Research Initiative (MURI) Airforce, Basic Energy Sciences (BES) Department of Energy (DOE) (No. DE-FG02-07ER46394) and the Knowledge Innovation Program of the Chinese Academy of Sciences (Grant No. KJCX2-YW-M13).

Electronic Supplementary Material: Reproducibility and stability of the GaN NB-based PDs are available in the online version of this article at http://dx.doi.org/10.1007/s12274-013-0354-2.

References

[1] Razeghi, M.; Rogalski, A. Semiconductor ultraviolet detectors. *J. Appl. Phys.* **1996**, *79*, 7433.

[2] Prasai, D.; John, W.; Weixelbaum, L.; Krüger, O.; Wagner, G.; Sperfeld, P.; Nowy, S.; Friedrich, D.; Winter, S.; Weiss, T. Highly reliable silicon carbide photodiodes for visible-blind ultraviolet detector applications. *J. Mater. Res.* **2013**, *28*, 33–37.

[3] Hochedez, J. F. E.; Schuehle, U. H.; Pau, J. L.; Alvarez, J.; Hainaut, O.; Appourchaux, T. P.; Auret, F. D.; Belsky, A.; Bergonzo, P.; Castex, M. C. et al. New UV detectors for solar observations. In *Proceedings of Innovative Telescopes and Instrumentation for Solar Astrophysics*, Hawai'i, USA, 2002, pp 419–426.

[4] Fernandez-Saldivar, J. A.; Underwood, C. I.; Mackin, S. Low-cost microsatellite UV instrument suite for monitoring ozone and volcanic sulphur dioxide. In *Remote Sensing of Clouds and the Atmosphere XI*, Stockholm, Sweden, 2006, pp 63621.

[5] Chen, Q.; Khan, M. A.; Sun, C. J.; Yang, J. W. Visible-blind ultraviolet photodetectors based on GaN p-n junctions. *Electron Lett.* **1995**, *31*, 1781–1782.

[6] Van Hove, J. M.; Chow, P. P.; Hickman, R.; Wowchak, A. M.; Klaassen, J. J.; Polley, C. J. Visible blind UV GaN photovoltaic detector arrays grown by rf atomic nitrogen plasma MBE. In *MRS Fall Meeting*, 1996, pp 12271–1232.

[7] Van Hove, J. M.; Hickman, R.; Klaassen, J. J.; Chow, P. P.;

Ruden, P. P. Ultraviolet-sensitive, visible-blind GaN photodiodes fabricated by molecular beam epitaxy. *Appl. Phys. Lett.* **1997**, *70*, 2282–2284.

[8] Osinsky, A.; Gangopadhyay, S.; Yang, J. W.; Gaska, R.; Kuksenkov, D.; Temkin, H.; Shmagin, I. K.; Chang, Y. C.; Muth, J. F.; Kolbas, R. M. Visible-blind GaN Schottky barrier detectors grown on Si(111). *Appl. Phys. Lett.* **1998**, *72*, 551–553.

[9] Walker, D.; Saxler, A.; Kung, P.; Zhang, X.; Hamilton, M.; Diaz, J.; Razeghi, M. Visible blind GaN p-i-n photodiodes. *Appl. Phys. Lett.* **1998**, *72*, 3303–3305.

[10] Misra, M.; Moustakas, T. D.; Vaudo, R. P.; Singh, R.; Shah, K. S. Photoconducting ultraviolet detectors based on GaN films grown by electron cyclotron resonance molecular beam epitaxy. In *Proceedings of the X-ray and Ultraviolet Sensors and Applications*, San Diego, USA, 1995, pp 78–86.

[11] Khan, M. A.; Shur, M. S.; Chen, Q.; Kuznia, J. N.; Sun, C. J. Gated photodetector based on GaN/AlGaN heterostructure field-effect transistor. *Electron Lett.* **1995**, *31*, 398–400.

[12] Lim, B. W.; Chen, Q. C.; Yang, J. Y.; Khan, M. A. High responsitivity intrinsic photoconductors based on $Al_xGa_{1-x}N$. *Appl. Phys. Lett.* **1996**, *68*, 3761–3762.

[13] Munoz, E.; Monroy, E.; Garrido, J. A.; Izpura, I.; Sanchez, F. J.; Sanchez-Garcia, M. A.; Calleja, E.; Beaumont, B.; Gibart, P. Photoconductor gain mechanisms in GaN ultraviolet detectors. *Appl. Phys. Lett.* **1997**, *71*, 870–872.

[14] Khan, M. A.; Kuznia, J. N.; Olson, D. T.; Blasingame, M.; Bhattarai, A. R. Schottky-barrier photodetector based on Mg-doped *p*-type GaN films. *Appl. Phys. Lett.* **1993**, *63*, 2455–2456.

[15] Chen, Q.; Yang, J. W.; Osinsky, A.; Gangopadhyay, S.; Lim, B.; Anwar, M. Z.; Khan, M. A.; Kuksenkov, D.; Temkin, H. Schottky barrier detectors on GaN for visible-blind ultraviolet detection. *Appl. Phys. Lett.* **1997**, *70*, 2277–2279.

[16] Binet, F.; Duboz, J. Y.; Laurent, N.; Rosencher, E.; Briot, O.; Aulombard, R. L. Properties of a photovoltaic detector based on an n-type GaN Schottky barrier. *J. Appl. Phys.* **1997**, *81*, 6449–6454.

[17] Smith, G. A.; Estes, M. J.; Van Nostrand, J. E.; Dang, T.; Schreiber, P. J.; Temkin, H.; Hoelscher, J. UV Schottky-barrier detector development for possible air force applications. In *Proceedings of the Photodetectors: Materials and Devices IV*, San Jose, USA, **1999**, pp 184–192.

[18] Kung, P.; Walker, D.; Sandvik, P. M.; Hamilton, M.; Diaz, J. E.; Lee, I. H.; Razeghi, M. Schottky MSM photodetectors on GaN films grown on sapphire by lateral epitaxial overgrowth. In *Proceedings of the Photodetectors: Materials and Devices IV*, San Jose, USA, **1999**, pp 223–229.

[19] Yu, R. M.; Dong, L.; Pan, C. F.; Niu, S. M.; Liu, H. F.; Liu, W.; Chua, S.; Chi, D. Z.; Wang, Z. L. Piezotronic effect on the transport properties of GaN nanobelts for active flexible electronics. *Adv. Mater.* **2012**, *24*, 3532–3537.

[20] Wang, Z. L. Progress in piezotronics and piezo-phototronics. *Adv. Mater.* **2012**, *24*, 4632–4646.

[21] Yang, Q.; Wang, W. H.; Xu, S.; Wang, Z. L. Enhancing light emission of ZnO microwire-based diodes by piezo-phototronic effect. *Nano Lett.* **2011**, *11*, 4012–4017.

[22] Yang, Q.; Liu, Y.; Pan, C. F.; Chen, J.; Wen, X. N.; Wang, Z. L. Largely enhanced efficiency in ZnO nanowire/p-polymer hybridized inorganic/organic ultraviolet light-emitting diode by piezo-phototronic effect. *Nano Lett.* **2013**, *13*, 607–613.

[23] Pan, C. F.; Niu, S. M.; Ding, Y.; Dong, L.; Yu, R. M.; Liu, Y.; Zhu, G.; Wang, Z. L. Enhanced Cu_2S/CdS coaxial nanowire solar cells by piezo-phototronic effect. *Nano Lett.* **2012**, *12*, 3302–3307.

[24] Zhang, Y.; Yang, Y.; Wang, Z. L. Piezo-phototronics effect on nano/microwire solar cells. *Energy Environ. Sci.* **2012**, *5*, 6850–6856.

[25] Yu, R. M.; Pan, C. F.; Wang, Z. L. High performance of ZnO nanowire protein sensors enhanced by the piezotronic effect. *Energy Environ. Sci.* **2013**, *6*, 494–499.

[26] Pan, C. F.; Yu, R. M.; Niu, S. M.; Zhu, G.; Wang, Z. L. Piezotroniceffect on the sensitivity and signal level of Schottky contacted proactive micro/nanowire nanosensors. *ACS Nano* **2013**, *7*, 1803–1810.

[27] Liu, H. F.; Liu, W.; Chua, S. J.; Chi, D. Z. Fabricating high-quality GaN-based nanobelts by strain-controlled cracking of thin solid films for application in piezotronics. *Nano Energy* **2012**, *1*, 316–321.

[28] Yang, R. S.; Qin, Y.; Dai, L. M.; Wang, Z. L. Power generation with laterally packaged piezoelectric fine wires. *Nat. Nanotechnol.* **2009**, *4*, 34–39.

[29] Zhang, Y.; Liu, Y.; Wang, Z. L. Fundamental theory of piezotronics. *Adv. Mater.* **2011**, *23*, 3004–3013.